Earth Syst. Dynam. Discuss., 6, 2137–2179, 2015
www.earth-syst-dynam-discuss.net/6/2137/2015/
doi:10.5194/esdd-6-2137-2015

Earth System Dynamics Discussions
Open Access
EGU

Importance of open-water ice growth and ice concentration evolution: a study based on FESOM-ECHAM6

X. Shi and G. Lohmann

Alfred Wegener Institute, Helmholtz Center for Polar and Marine Research, Bussestr. 24, 27570 Bremerhaven, Germany

Received: 13 October 2015 – Accepted: 20 October 2015 – Published: 28 October 2015

Correspondence to: X. Shi (xshi@awi.de)

Published by Copernicus Publications on behalf of the European Geosciences Union.

Abstract

A newly developed global climate model FESOM-ECHAM6 with an unstructured mesh and high resolution is applied to investigate to what degree the area-thickness distribution of new ice formed in open water affects the ice and ocean properties. A sensitivity experiment is performed which reduces the horizontal-to-vertical aspect ratio of open-water ice growth. The resulting decrease in the Arctic winter sea-ice concentration strongly reduces the surface albedo, enhances the ocean heat release to the atmosphere, and increases the sea-ice production. Furthermore, our simulations show a positive feedback mechanism among the Arctic sea ice, the Atlantic Meridional Overturning Circulation (AMOC), and the surface air temperature in the Arctic, as the sea ice transport affects the freshwater budget in regions of deep water formation. A warming over Europe, Asia and North America, associated with a negative anomaly of Sea Level Pressure (SLP) over the Arctic (positive phase of the Arctic Oscillation (AO)), is also simulated by the model. For the Southern Ocean, the most pronounced change is a warming along the Antarctic Circumpolar Current (ACC), especially for the Pacific sector. Additionally, a series of sensitivity tests are performed using an idealized 1-D thermodynamic model to further investigate the influence of the open-water ice growth, which reveals similar results in terms of the change of sea ice and ocean temperature. In reality, the distribution of new ice on open water relies on many uncertain parameters, for example, surface albedo, wind speed and ocean currents. Knowledge of the detailed processes is currently too crude for those processes to be implemented realistically into models. Our sensitivity experiments indicate a pronounced uncertainty related to open-water sea ice growth which could significantly affect the climate system.

ESDD
6, 2137–2179, 2015

1 Introduction

Sea ice is one of the most visible indicators of our changing climate owing to its reflecting and isolating properties (IPCC, 2013). On one hand, sea ice reflects part of the incoming solar radiation due to its high surface albedo; on the other hand, sea ice reduces the heat exchange between the atmosphere and the ocean. Therefore, the concentration of sea ice regulates the air-ocean interaction and thus plays an important role in the climate system. It has been argued that a reduction in the high-latitude ice concentration has impacts on the atmosphere and ocean characteristics (e.g., Royer et al., 1990; Deser et al., 2010; Semmler et al., 2012). For example, Deser et al. (2010) used an atmospheric general circulation model (CAM3) to investigate the atmospheric response to projected Arctic sea ice loss at the end of the 21st century, and found an increase in snowfall over North America, Asia and the northern part of Europe. Semmler et al. (2012) used the atmospheric general circulation model EC-EARTH-IFS to carry out sensitivity experiments with reduced ice cover, and found negative sea level pressure anomalies over the western Arctic and positive anomalies over Siberia, affecting surface temperatures over Europe. An extreme scenario experiment with no Arctic sea ice in winter was conducted by Royer et al. (1990) using an atmosphere stand-alone model,they found strongly enhanced surface latent and sensible heat fluxes in winter, and corresponding effects on temperature and circulation.

Given these results, there is no doubt that ice concentration is crucial to any realistic modeling of the Earth's climate. Changes in sea ice conditions are affected by processes involving complex feedback mechanisms, such as ocean-atmosphere interactions, surface albedo and desalination processes of sea ice. Since some processes related to sea ice conditions are too complicated or not sufficiently understood to be resolved by the models' governing equations, it is necessary to apply parameterizations to empirically describe such processes. However, the representation of some of these factors in numerical models is still subject to large uncertainties (e.g., Notz, 2012). One of these uncertain parameterizations is the open-water ice growth, which is a key el-

ESDD
6, 2137–2179, 2015

ement contributing to sea ice concentration. During the ice accretion period, new ice volume generated on open water is distributed into growth in vertical and horizontal directions, contributing to both ice thickness and concentration. So far much effort has been made to simulate open-water ice growth. Hibler (1979) introduced a demarcation between thin and thick ice at $h_0 = 0.5$ m. It is assumed that in the freezing case, the fraction of open water is allowed to decay exponentially with a time constant of $h_0/\dot{h}_{ow}$, with $\dot{h}_{ow}$ being the growth rate of ice on open water. Reasoning and sensitivity studies were presented by Mellor and Kantha (1989), who suggested an aspect ratio of $\Phi_F = 4$ to divide open-water ice growth between increase in ice thickness and in ice area. Dorn et al. (2009) parameterize the increase rate of ice concentration due to freezing on open water based on a reference thickness for lateral melting. In a similar way, Vancoppenolle et al. (2009) used a thickness of $0.05 < h_0 < 0.15$ m in the model LIM3 to limit new ice in open water when transforming new ice volume to thickness and concentration. However, it is a great challenge to simulate the open-water ice growth since this process is only partly understood and currently not realistically represented in models (Notz, 2012), therefore there is room for calibration and improvement. The new ice formed on open water can be parameterized as in the left panel of Fig. 1 (with relatively less thickness and more concentration) or as the right panel (with more thickness but less concentration, i.e., more open water).

The main purpose of this study is to investigate to what extent the lateral-vertical ice growth ratio within open water can affect the simulation results, which has only been done mostly in stand-alone sea ice models (e.g., Hibler, 1979; Fichefet and Maqueda, 1997; Biggs et al., 2000; Wang et al., 2010; Smedsrud, 2011). For example, when the aspect ratio is large enough for producing a lead-free ice region, a drastical reduction in sea ice volume is given by the LIM2 model (Fichefet and Maqueda, 1997). Using the same model, Wang et al. (2010) reveals simple relations between ice conditions and the lateral-vertical ice growth ratio.

In the present paper, we reduce the horizontal ice accretion on open water in a coupled climate model FESOM-ECHAM6 (Sidorenko et al., 2014) and an idealized

ESDD
6, 2137–2179, 2015

1-D model. In this way, when ice forms over sea water, the added ice concentration becomes smaller, while, the increase in ice thickness is larger (Fig. 1).

A brief introduction of the parameterization of ice cover evolution used in FESOM-ECHAM6 is presented in Sect. 2. Detailed information about the coupled model and idealized 1-D model, as well as our experimental design, are described in Sect. 3. Section 4 deals with the results of the circulation model as well as sensitivity tests from the 1-D model. Section 5 provides a discussion and Sect. 6 gives the conclusions of this study.

2 Parameterization of ice concentration evolution

There are two main thermodynamic processes relating to changes in sea ice concentration: (1) freezing occurs on open water when sea water at its freezing point is cooled by the atmosphere, which reduces the open water area; (2) melting of sea ice (including both vertical and lateral melt) leads to a decrease in ice concentration (Hibler, 1979). Furthermore, there are also some dynamic processes, such as divergence and ridging, that can affect the ice concentration evolution, which is however beyond the scope of our study. The infomation about the variables and parameters in this paper are listed in Table 1.

Here, we briefly introduce the parameterization of ice concentration evolution used in FESOM-ECHAM6 which is described in Dorn et al. (2009). Firstly, when new ice is formed on open water, the ice concentration increases at a rate given by:

$$\dot{A}_{\mathrm{ow}} = \frac{1}{h_0}\max(\dot{h}_{\mathrm{ow}}, 0) \tag{1}$$

where $\dot{h}_{\mathrm{ow}}$, the effective ice production rate at open water area, is calculated based on the open water energy budget:

$$\dot{h}_{\mathrm{ow}} = (1 - A) \times \frac{\max(F_{\mathrm{atmocn}}, 0)}{\rho_i L} \tag{2}$$

ESDD
6, 2137–2179, 2015

The lead closing parameter h_0 in the equation is computed by:

$$h_0 = \max({h_0}^{\min}, \min({h_0}^{\max}, h)) \tag{3}$$

According to Dorn et al. (2009), ${h_0}^{\min}$ and ${h_0}^{\max}$ are set to 0.5 and 1.5 m, respectively, h stands for the grid-cell mean ice thickness, i.e., the ice volume divided by the area of the gird cell.

It is assumed that the ice thickness on a subgrid-scale is linearly distributed between 0 and $2h'$ (h' represents the actual sea ice thickness) (Hibler, 1979), when sea ice melts vertically, the ice concentration decreases at a rate of

$$\dot{A}_{\text{ice}} = \frac{1}{2h'} \min(\dot{h}_{\text{ice}}, 0) \tag{4}$$

The actual ice thickness h' is computed as $h' = h/A$, i.e., effective ice thickness h divided by ice concentration A. $\dot{h}_{\text{ice}}$ is the thermodynamic ice production rate of the sea-ice fraction, which is represented by:

$$\dot{h}_{\text{ice}} = A \times \frac{F_{\text{atmice}} - F_{\text{ocnice}}}{\rho_i L} \tag{5}$$

For more detailed information, we refer to Dorn et al. (2009).

In the present paper, we multiply $\dot{A}_{\text{ow}}$ by a factor c_* ($c_* = 80\,\%$) to alter the horizontal-to-vertical aspect ratio of ice growth during the freezing period of open-water, as in

$$\dot{A}_{\text{ow(new)}} = \dot{A}_{\text{ow}} c_* \tag{6}$$

By performing such modification, the lateral ice growth within open water is decreased. Taking into account the mass conservation, the actual sea ice thickness is automatically adjusted by the model. Sea ice formed in this new method is “narrower” and “thicker” (Fig. 1) than it is in the original parameterization (i.e., Eq. 1).

ESDD
6, 2137–2179, 2015

3 Models and experimental design

3.1 FESOM-ECHAM6

FESOM-ECHAM6 is a newly developed global coupled climate model (Sidorenko et al., 2014) which has been established at the Alfred Wegener Institute (AWI). The ocean and sea ice component is the Finite Element Sea Ice-Ocean Model (FESOM) (Danilov et al., 2004; Timmermann et al., 2009; Sidorenko et al., 2011; Wang et al., 2013; Sidorenko et al., 2014) which is discretized on a triangular grid with a continuous conforming representation of model variables, whereas the atmospheric module is represented by the general circulation model ECHAM6 (Stevens et al., 2013).

The sea ice component is a dynamic-thermodynamic sea ice model with the Parkinson and Washington (1979) thermodynamics. The model consists of subgrid-scale processes based on Redi (1982), a so-called zero-layer approach of Semtner (1976) and a submodel of ice dynamics according to an elastic-viscous-plastic rheology (Hunke and Dukowicz, 1997). When calculating the growth rate of ice in ice covered parts, the model assumes that ice thickness has an equal, seven-category distribution from zero to two times ice thickness, following Hibler (1979). The model also includes a prognostic snow layer (Owens and Lemke, 1990). The paramerization of snow-ice conversion is based on Leppäranta (1983). The sea ice model has been validated in Timmermann et al. (2009) and Scholz et al. (2013).

To be more specific about the thermodynamic process of the sea ice, FESOM-ECHAM6 computes ice growth on ice part and open-water part separately (Parkinson and Washington, 1979; Dorn et al., 2009), the changed ice thickness in each part is then weighted by the ice concentration and water fraction, respectively, to obtain the mean change in ice thickness in the grid cell (see Eqs. 2 and 5). Increasing and decreasing ice concentration are calculated by the parameterization described in Sect. 2 (see Eqs. 1 and 4).

A T63 grid (about $1.9^{\circ} \times 1.9^{\circ}$) with 47 vertical levels is applied in the atmosphere component ECHAM6. In terms of the ocean module, FESOM uses a varying resolution

ESDD
6, 2137–2179, 2015

from about 200 km in the open ocean to 20 km along coastlines (Fig. 2), with 40 309 nodes on the surface. There are 46 vertical levels for the ocean.

3.2 Simple Idealized Model (SIM)

To conduct sensitivity studies and to examine the impact of horizontal-to-vertical open-water ice growth ratio on ice and ocean properties in an idealized setup, a simple 1-D thermodynamic sea-ice model (hereafter referred to as the SIM) including an ocean mixed layer is introduced.

The SIM uses a zero-layer approach (Semtner, 1976), where the ice surface temperature T_s is determined by the heat balance at the ice-atmosphere interface:

$$-(1-\alpha)F_{sw} - F_{other} + \varepsilon\sigma {T_s}^4 = -k_i \frac{T_s - T_{bot}}{h}. \quad (7)$$

Here, α is the albedo of the ice surface, which is calculated based on the measurements obtained during the SHEBA campaign (Perovich et al., 1999):

$$\alpha = \frac{-0.431}{1 + (\frac{d-207}{44.5})^2} + 0.914,$$

with d being the number of the day in the year (ranging from 1 to 365), F_{sw} the shortwave flux and F_{other} the sum of sensible heat flux, latent heat flux and downwelling longwave radiation. The third term in Eq. (7) stands for the thermal radiation flux released by the ocean surface, where T_s is the surface temperature, $\varepsilon = 0.97$ represents the emissivity coefficient, and $\sigma = 5.67 \times 10^{-8}\,\mathrm{Wm^{-1}\,K^{-4}}$ is the Stefan–Boltzmann constant.

The seasonal variation of the atmospheric fluxes F_{sw} and F_{other} (in $\mathrm{W\,m^{-2}}$) are prescribed as:

$$F_{sw} = 19.5 \times \exp\left[-0.5 \times \left(\frac{d - 164.1}{47.9}\right)^2\right] \times 16.1 \quad (8)$$

ESDD
6, 2137–2179, 2015

$$F_{\text{other}} = 117.8 \times \exp\left[-0.5 \times \left(\frac{d - 206}{53.1}\right)^2\right] \times 179.1 \quad (9)$$

These two equations match the monthly-mean data compiled by Maykut and Untersteiner (1971).

In FESOM, the surface heat balance equation is similar to Eq. (7) but is more complex. The elements determining the ice-ocean interface temperature involve the albedo, solar radiation, sensible and latent heat flux, the emissive long wave radiation from the surface to atmosphere, sea ice change, snow sublimation, precipitation, evaporation and river runoff. Radiative fluxes in FESOM are not empirically determined as in SIM, but based on the atmospheric and oceanic state.

To be consistent with FESOM-ECHAM6, the SIM calculates ice growth/melt rate over sea ice ($\dot{h}_{\text{ice}}$) and open water ($\dot{h}_{\text{ow}}$) by Eqs. (5) and (2), and the corresponding change in ice concentration by Eqs. (4) and (1).

An idealized mixed layer (depth, h_{mix}), which can store and release heat, is coupled to the model via the oceanic heat flux F_{ocnice}:

$$F_{\text{ocnice}} = -\rho_{\text{w}} c_{\text{w}} \gamma_{\text{t}} (T_{\text{mix}} - T_{\text{f}}), \quad (10)$$

where F_{ocnice} is the heat flux at the ice-ocean interface, ρ_{w} the water density, c_{w} the specific heat capacity of sea water, T_{mix} and T_{f} the temperature of mixed-layer and freezing point, respectively. Here we assume the heat transfer speed γ_{t} to be 10 m per day (i.e., $\gamma_{\text{t}} = 10/86\,400\,\text{m s}^{-1}$), which is consistent with FESOM-ECHAM6.

3.3 Experimental design

In the following section we describe the experimental setup of seven simulations. A summary of the experiment characteristics is also provided in Table 2.

Using the circulation model FESOM-ECHAM6 we perform two experiments FE-CTR and FE80, which are both initialized from a 300 years' spin-up under pre-industrial

ESDD
6, 2137–2179, 2015

boundary conditions (Berger, 1978; Crucifix et al., 2005). Experiment FE-CTR uses Eq. (1) to calculate the horizontal growth rate of ice during open-water ice formation, while Eq. (6) is applied in FE80 with c_* being 80 %. Both experiments are integrated for 50 years. The average of the model years 31–50 is considered to represent the climatology in both simulations.

Five SIM model experiments, each lasting 50 years, are carried out to examine the effect of c_* in an idealized thermodynamic setup, and to test the sensitivity of the model's solution to changes in the value of c_*, which varies from 20 to 80 %. The output of the last 20 model years is used for analysis.

4 Results

4.1 Result of FESOM-ECHAM6

a. Climatological sea ice

Figure 3 provides a seasonal picture of mean ice thickness conditions throughout the Arctic. It clearly shows areas of thick ice floes (mean thickness larger than 5 m) over the north side of Greenland and the Canadian Archipelago. Such pattern is mainly due to the Beaufort Gyre and Transpolar Drift Stream which tend to push the ice pack around the Arctic Ocean in a clockwise direction, causing the ice to the north to pile up along the natural barriers to this flow. The thick-to-thin ice gradient is clearly captured by the model from the Canadian Archipelago (5 m) towards the Siberian coast (less than 1 m). In September, the sea ice significantly retreats from subpolar North Atlantic and Bering Strait to the Arctic Basin north of 50° N. It is obvious that Southern Ocean sea ice is generally thinner than its counterpart in the Arctic. In the model simulations, most Southern Ocean ice is thinner than 2 m. In March, the sea ice only occupies the Weddell Sea and Antarctic coastal regions, while in September the sea ice extends further to 60° S.

ESDD
6, 2137–2179, 2015

Figure 4 presents the mean sea-ice concentration of the model in FE-CTR. The Arctic sea ice in winter reveals a large coverage over the entire central Arctic region. The 15 % boundary of the winter sea-ice concentration extends into the Barents Sea up to 75° N, and along the east coast of Greenland and the Labrador Peninsula up to 53° N. The pronounced retreat in the summer Arctic sea-ice coverage is clearly seen. The sea ice cover is overestimated in the Arctic summer due to a local cooling in the lower atmosphere (Sidorenko et al., 2014). The ice concentration over the Southern Ocean reaches its maximum along the coastal regions of Antarctic continent and minimum in the Marginal Ice Zone (MIZ).

b. Changes in ice thickness and ice concentration

Compared to FE-CTR, there is an increase in sea ice thickness in FE80 over the entire Arctic (Fig. 5a–c), with the maximum change of about 0.8 m occurring over the coastal region north of Greenland, where sea ice reaches its maximal thickness. The reason for such pronounced change likely lies on a local cooling over the Greenland-Iceland-Norwegian (GIN) Sea and the ice mass transport by the clockwise Beaufort Gyre. Similarly, decreasing the value of $\dot{A}_{ow}$ in the Southern Hemisphere yields a general enhanced production of sea ice (Fig. 5d–f), the difference amounts approximately to 0.3 m over coastal region of the Antarctic continent, and to less amount for the areas which are relatively far from the continental shelf.

Figure 6 displays the changes of sea ice concentration. In most regions of the Arctic and subpolar areas, we observe slight decrease and increase of sea ice concentration in March and September, respectively. This is reasonable, as the open-water ice growth mostly takes place in cold months, the reduced $\dot{A}_{ow}$ directly leads to decreased ice concentration and increased ice thickness in boreal winter. The resulting thicker sea ice persists longer on the sea surface during melting period, thereby reducing the areas of open water and leads in summer. Besides, a more pronounced feature is the increase in sea ice concentration in the marginal ice zone, i.e., the Bering Sea and North Atlantic subpolar gyre (Fig. 6a). Similarly, the sea ice concentration decreases for most parts

ESDD
6, 2137–2179, 2015

of the Southern Ocean during austral winter (September) which dominates its annual pattern. Whereas, positive anomalies of sea ice concentration are found along the Antarctic continental shelf in austral summer (March).

c. Changes in the sea surface temperature and salinity

Figure 7a depicts the responses of the sea surface temperature (SST). Compared to FE-CTR, pronounced cooling is simulated over the GIN Sea and the North Atlantic in FE80, with the most significant change (over −1 °C) occurring at the North Atlantic subpolar gyre, while for the Southern Ocean it is the opposite case, with the strongest warming happening at the region of Antarctic Circumpolar Current (ACC) (about 0.5 °C).

The simulated changes in the sea surface salinity (SSS) show a more saline central Arctic (Fig. 7b), as a consequence of the enhanced brine release led by sea ice production. However, in the GIN Sea, freshening occurs in spite of the increase in sea ice volume. We attribute this phenomenon to a sea ice dynamic process: enhanced sea ice import through Fram Strait, that affects the freshwater budget of the GIN region.

To further investigate the impact of Arctic sea ice transport on the deep water formation, composite analyses are calculated as depicted in Fig. 8, by averaging the SSS anomaly fields that have more than one standard deviation with respect to indices of the Fram Strait ice mass import. A pronounced freshening happens over the subpolar North Atlantic Ocean as a result of the Fram Strait ice mass import, with a delay of 4 years. Such pattern is similar to the SSS anomalies which is shown in Fig. 7b. The resulting less dense sea water leads to a weakened downwelling current over the North Atlantic and a decline in AMOC circulation.

d. Positive feedback behind the sea ice change in the Arctic

In boreal winter, new sea ice is formed on open water when the ocean loses heat to atmosphere and the temperature of sea water is about to fall below its freezing point.

ESDD
6, 2137–2179, 2015

As a result of reduced $\dot{A}_{ow}$, sea ice grows more in the vertical direction, increasing the persistence of open water in boreal winter (Fig. 6a) and the accompanying heat loss from ocean to air. More sea ice is therefore generated which in turn helps to increase the sea ice thickness as depicted in Fig. 5a–c. Much of the thicker sea ice persists during summer, leading to higher ice concentration in September (Fig. 6b).

Figure 9 represents the effect of reduced $\dot{A}_{ow}$ on the thermodynamic growth of sea ice. Obvious negative patterns are observed at the GIN Sea, Labrador Sea and the Atlantic subpolar gyre, despite the increase in sea-ice thickness and concentration there. Therefore, the enhanced sea ice production in those regions is not owing to local ice thermodynamic growth. As the increased sea ice in the Arctic strongly reinforces sea ice export into the subpolar regions through Fram Strait. Such process is captured in the anomalies of ice mass transport as illustrated in Fig. 10. The increased sea ice in GIN Sea, Labrador Sea and the Atlantic subpolar gyre is affected by the stronger Fram Strait sea ice import.

In boreal summer, the ablation of sea ice at the GIN Sea reduces both the surface temperature and salinity of that region, and further affects the North Atlantic Ocean. Figure 11a, b represent the changes of zonal profiles of the ocean temperature and salinity. In FE80, there is generally a decrease in water temperature compared to FE-CTR for the upper ocean (0–100 m), at the same time, the sub-surface signal between 100–1000 m shows the opposite behavior. Fresher sea water is simulated in FE80 for the upper ocean (0–100 m) of 30–65° N latitude, and the opposite pattern is the case for the Arctic surface and sub-surface. The weakening of the AMOC (Fig. 11c) is owing to the negative salinity anomaly which weakens the sinking in the North Atlantic Ocean. The spatial patterns of the surface air temperature (SAT) anomalies, associated with low phases of AMOC are illustrated by a composite map (Fig. 12). During the low phase of the AMOC, there is a general cooling of −0.5 °C in the central Arctic Ocean. A more pronounced feature is the cooling over the North Atlantic Ocean, with a magnitude of −1 °C, which is associated with the weakened surface northward heat transport during years with low AMOC. Therefore, the decrease in AMOC leads to a general decrease

ESDD
6, 2137–2179, 2015

in the Arctic SAT, which in turn increases the Arctic sea ice. In this way, a positive feedback is formed (Fig. 13).

In summary, the Arctic grid-cell mean sea-ice thickness in FE80 increases as a result of the reduced $\dot{A}_{ow}$ and the stronger air-sea interaction in winter through larger open-water and leads. The increase in sea-ice volume leads to an enhanced ice transport towards the subpolar regions through Fram Strait, which increases the ice thickness and cover there. In the ablation period, sea ice melts and freshens the North Atlantic Ocean, thus weakening the Atlantic overturning circulation. As a result, the associated Arctic SAT tends to decrease, allowing more sea ice formation, which in turn helps to reinforce the ice transport and freshens the North Atlantic Ocean (Fig. 7b).

e. Mechanism for the sea ice change in the Southern Ocean

Different from the Arctic sea ice, the sea ice in the Southern Ocean is seasonal rather than multi-year, therefore shows more pronouced response to change of open-water ice growth parameterization. Increased open-water and leads in austral winter (September) results in enhanced sea ice growth, which buffers the effect of the reduced $\dot{A}_{ow}$ on sea ice concentration. Thicker sea ice persists longer in austral summer, which is the reason why the sea ice concentration generally increases in March.

In contrast to the cooling of the North Atlantic, most parts of the Southern Ocean experience an increase in SST with the most significant warming occurring along the route of the ACC (about 0.5 °C). Such pattern is likely caused by processes involving stronger vertical mixing and enhanced convective overturning, which tends to bring warm circumpolar sea water to the surface. The ACC warming can be seen in all seasons throughout the year.

f. The surface air temperature and the Arctic Oscillation (AO)

Figure 14a shows the difference of SAT in boreal winter. A significant warming is simulated in FE80 compared to FE-CTR over Asia and North America (2 °C), and a less

ESDD
6, 2137–2179, 2015

pronounced warming is observed over Europe (0.5 °C). In the regions of Greenland, the Nordic Sea and Bering Sea, FE80 leads to a cooling surface, with a magnitude of about −2 °C. The SAT change of the GIN Sea and North Atlantic subpolar gyre, which is consistent with the ocean temperature difference there, is due to the large ice ablation in summer as described in Sect. 4.1b.

To explain such model behavior, we now turn to examine the sea level pressure (SLP) change in boreal winter (Fig. 14b). The most distinguished feature is a tri-polar pattern with a negative SLP anomaly over the high latitudes, and two positive SLP anomalies over the northern Pacific, and eastern part of North Atlantic together with south-western Europe, respectively, which forms an AO-like mode.

The warming over Europe and Asia can be explained by enhanced westerlies and thereby more heat transport from the North Atlantic, the same phenomenon is also found by Hurrell (1995). Similarly, the positive SLP anomaly over the northern Pacific brings relatively warmer air to North America.

4.2 Sensitivity tests by SIM

We now turn to investigate the impact of c_* (reduced $\dot{A}_{\mathrm{ow}}$) in an idealized setup (Fig. 15). SIM80 yields similar results in comparison to its FE80 conterpart for the Arctic Ocean: (1) the ice thickness increase, (2) there is no distinguishable change for the ocean temperature, and (3) ice concentration decreases in winter, but with a large magnitude (−5 %). However, the ice concentration change in SIM model shows a reduction all the year round, different from that in FESOM-ECHAM6, which reveals a slight decrease in ice concentration in boreal winter (less than −5 %) and an increase in boreal summer.

By applying even smaller c_* (or $\dot{A}_{\mathrm{ow}}$), the above differences are more pronounced in FE60 and FE40, except that the freeze-up date is much later than the control experiment, leading to thinner sea ice in winter, even though sea ice grows more rapidly in sensitivity simulations in winter.

ESDD
6, 2137–2179, 2015

For an extreme case of $c_* = 20\,\%$ (SIM20), a much warmer ocean is simulated as larger parts of open water appears in SIM20 compared to that in SIM-CTR. As a consequence, sea ice rapidly melts in summer, leading to an ice-free ocean two months earlier than SIM-CTR, and the beginning day of ice-formation is delayed to the next year. As a consequence, the sea ice in SIM20 is the thinnest among all SIM simulations.

The above experiments reveal a robust sensitivity of model simulated sea ice thickness and concentration to changes in c_*. We note that c_* in the climate model FESOM-ECHAM6 is a sensitive parameter for the mean sea ice and AMOC climatology. We deliberately refrain from tuning the model's solution for different c_*. As the main objective of this study is to understand the importance of open-water ice growth to the simulated climate, seeking for the optimal values of c_* is beyond the scope of this study.

5 Discussion

FESOM is a high-resolution ice-ocean model which has the advantage of providing a regional focus in an otherwise global setup (Sidorenko et al., 2011). In our work, FESOM applies even higher resolution in the high latitudes than the tropical and subtropical region. It is therefore suitable for investigating polar properties, particularly sea ice characteristics, and the related processes.

As reported by Notz (2012), so far, focus of sea ice simulation has been solely on changes in the ice volume that result from changes in the ice thickness. However, for a realistic representation of the impact of thermodynamics on sea-ice thickness distribution, its lateral versus vertical heat exchange – including the open water ice growth and lateral/vertical ice accretion – is also of importance on ice extent, in particular on simulations extending beyond a few days. Ice growth on open water is a key element of any sea-ice model (Hibler, 1979). The new ice volume formed on open water is transferred into solid sea ice which limits the area of open water as well as heat exchange between the water and the air. A difficulty arises when distributing the new ice volume

ESDD
6, 2137–2179, 2015

between growth in area and thickness (Smedsrud, 2011). It should be noted that with the presence of a thin ice cover (normally below 20 cm) the ocean-atmosphere heat exchange still occurs (Maykut, 1986).

Unfortunately, this process cannot be explicitly resolved in large-scale models and needs to be parameterised. Through sensitivity experiments with the LIM2 sea-ice model, Fichefet and Maqueda (1997) indicated that when the model was run without leads, the air-sea heat fluxes were substantially modified, resulting in drastically reduced sea-ice thickness and total ice volume. Biggs et al. (2000) introduced a more physically based parameterisation of open water ice formation with the lead closing parameter h_0 being a nonlinear function of ice velocity, wind speed and packice thickness. Vancoppenolle et al. (2009) reported that the computed values of h_0 are well-suited for the simulation of new ice growth in the calm waters of the Arctic Ocean, as well as for leads and polynyas. Furthermore, Wang et al. (2010) indicated that the increase in h_0 leads to decreased ice concentration during ice growth, and the annual mean sea ice volume, thickness and extent all increase with h_0, which is in good consistency with our results.

In sea ice models, the volume of new ice can be computed from the open water energy budget, then difficulties and uncertainties arise when transforming the certain volume of new ice into growth in thickness and concentration in that grid cell. It is not known how the new ice shall be distributed in reality. Our purpose is to investigate to what extent such parameter can affect the simulation results. We do observe significant changes of sea ice, ocean and even the climate when changing this parameter, and the changes to sea ice and AMOC are mostly beyond internal variability of the model.

New ice formation strongly depends on many uncertain parameters, such as wind speed (Alam and Curry, 1998; Winsor and Björk, 2000; Smedsrud and Skogseth, 2006), ocean currents (Kämpf and Backhaus, 1999), ice velocity and packice thickness, and is based on a theoretical polynya model (Biggs et al., 2000), which was validated with laboratory work (Martin and Kaufmann, 1981). One could describe the factor c_* as a function of these elements. The newly formed sea ice then in turn affects these sea

ESDD
6, 2137–2179, 2015

state variables, which can further cause discrepancies in some regional parts. Therefore, one can expect that the anomalies of ice, ocean and surface properties observed in our work, are owing to the combined effects of all the processes mentioned above. Even though seeking for the optimal values of c_* is beyond the scope of this study, we can empirically determine a factor c_* to reduce the discrepancy between observed and modeled sea ice evolution. FESOM-ECHAM6 tends to overestimate the sea ice volume over the GIN Sea and subpolar North Atlantic (Sidorenko et al., 2014), we expect that such problem can be solved by applying a larger horizontal-to-vertical aspect ratio of open-water ice growth ($c_* > 100\,\%$) over the Northern Hemisphere.

The most significant response to the increased lead closing parameter happens at sea ice edge rather than the central Arctic. This is mainly due to two factors: one is that the ice in the central Arctic has almost full ice coverage, and the effect of c_* can only take place on open water. Another reason is that, as described in Eqs. (1) and (2), when ice grows on open water, the increase in ice concentration is relatively larger for thinner ice, thus the factor c_* is more important for the ice boundary parts. Basically, the factor c_* only matters in autumn and winter when thermodynamic ice growth occurs. So the resulting reduction of ice concentration in SIM is an artifact dominated by the winter ice change. In our complex FESOM-ECHAM6, the summer ice concentration is also affected by other elements such as the ice dynamics, therefore the effect of c_* is overwhelmed.

Partitioning of lateral versus vertical growth of sea ice is most realistically simulated in models that explicitly include a sub-scale distribution of ice thickness (Bitz et al., 2001). In such models, lateral melting can roughly be represented by the disappearance of the thinnest sea-ice classes and the accompanying expansion of open water. However, in multi ice-thickness distribution model, the lead-closing parameter would still need to be determined empirically. Another realistic approach of lateral versus vertical melting is based on the ratio of bottom area versus edge area of the ice pack. However, the relationship between the ice floe size and many external factors, for example, ice age,

ESDD
6, 2137–2179, 2015

ice thickness and weather condition (Dumont et al., 2011) is not yet sufficiently very crudely implemented in sea ice models.

Regarding the relationship between the Arctic sea ice and AMOC (Fig. 13), a similar positive feedback has been also identified for hosing experiments in the North Atlantic Ocean (Lohmann and Gerdes, 1998), but without sea ice transport. In detail, more sea ice decreases the AMOC, which cools the high latitudes. Koenigk et al. (2009) found that the interannual variability of sea ice volume in the subpolar Arctic is mainly determined by variations in sea ice import from the Central Arctic. Here, we find that sea ice transport affects the freshwater budget in regions of deep water formation, and therefore affects the AMOC. As pointed out in several studies (e.g., Rühlemann et al., 2004; Knight et al., 2005; Zhang, 2007, 2008; Chylek et al., 2009), the AMOC has been linked to the Northern Hemisphere sea surface temperature (SST) and mid-depth temperature. The opposite trends in mid-depth warming and cooling in the downward branch of the North Atlantic deep water (Fig. 11) is consistent with projections and internal variability linked to the AMOC (Lohmann et al., 2008).

Besides ice and ocean properties, c_* can also have influences on the climate, as a pronounced warming over Eurasia and North America is observed in our sensitivity experiment, which results from a strengthening AO-like pattern. There are studies presenting the response of temperature to changes in SLP, which resemble our findings. For example, Hurrell (1995) has shown that negative SLP anomalies over Iceland and enhanced westerly flow are associated with positive temperature change extending from Great Britain and Scandinavia far into Siberia. Kodera and Yamazaki (1994); Graf et al. (1995); Kodera and Koide (1997) suggested a possibility of a dynamical linkage between the wintertime warming over Eurasia and enhanced polar night jet linked to AO+. Experiments with an atmospheric GCM (GFDL AM2) are used to determine the effect of the 1990s thinning of Arctic sea ice (Gerdes, 2006), the atmospheric response comprises a reduction in SLP in the central Arctic and over the Nordic Seas, and high pressure anomalies over the subtropical North Atlantic and the subpolar North Pacific. More recently, Semmler et al. (2012) forced the model EC-EARTH-IFS with reduced

ESDD
6, 2137–2179, 2015

ice cover, and found negative sea level pressure anomalies over the western Arctic and positive anomalies over Siberia, affecting surface temperatures over Europe.

It should be noted that our sensitivity experiment aims at changing the horizontal-to-vertical growth ratio of newborn ice on open water as shown in Fig. 1, and is not for simulating the climate changes. This study is motivated by the uncertainties in the parameterizations distributing the new ice volume between growth in area and thickness, which is due to our lack of fundamental understanding and a proper representation of processes in coupled simulations. However, a changed parameter in sea ice growth as done here could also affect the response of the system to past and future climate change scenarios, which is subject of a forthcoming study. Furthermore, this paper could be helpful for paleo-research and future climate projection. It is possible that in reality the factor c_* is climate dependent, and could be different under different climate conditions.

6 Conclusions

In the present paper, we conduct two model simulations in order to investigate the effects of the horizontal-to-vertical aspect ratio of open-water ice growth on sea ice, ocean and the climate. Compared to the reference experiment, FESOM-ECHAM6 results show a significant increase in ice thickness for the whole Arctic and some parts of the Southern Ocean in our sensitivity experiment. In the Arctic Ocean, a positive feedback among sea ice, AMOC and sea surface temperature is simulated: increase in sea ice thickness (i.e., ice volume) leads to more ice transport towards the GIN Sea. In spring and summer, ice melts and freshens the sea water at the GIN Sea and the North Atlantic subpolar gyre, thus weakening the AMOC. As a result, the associated SAT in the Arctic decreases, allowing more sea ice formation, which in turn helps to reinforce the ice transport and freshen the North Atlantic Ocean. Furthermore, warmer surface temperature in most parts of Eurasia and North America in boreal winter is simulated,

ESDD
6, 2137–2179, 2015

associated with positive SLP anomalies over the North Atlantic and North Pacific which contribute to increase the westerly winds from oceans to continents.

We perform similar experiments with an idealized 1-D model. Our results show a decrease in ice concentration as a direct consequence of the factor c_*, and an increase in ocean temperature owing to more air-sea interaction in summer through larger open water. In mid and late winter, the ocean loses more heat; therefore larger ice thickness is formed. During the ice melting period, higher temperatures of the ocean help to reduce the ice thickness. When ice begins to form in late autumn and early winter, ocean temperature in the sensitivity experiment reaches its freezing point several days later, thus the ice formation starts later but grows faster compared to that in the reference experiment. However, in an extreme case of $c_* = 20\,\%$, the ocean gets too warm, an ice-free ocean is simulated for most of the year.

The results presented in this study emphasize the importance of open-water ice growth. In detail, the distributing of new ice volume between growth in area and thickness can affect the ice properties, the ocean circulation and even the climate system in our climate model FESOM-ECHAM6. Another approach is a stochastic method (Juricke and Jung, 2014) to parameterize the open-water ice growth. Further analysis of the sea ice processes is necessary in order to test the robustness of climate change scenarios, especially at high latitudes where sea ice plays a dominant role.

Acknowledgements. We want to thank Dmitry Sidorenko, Patrick Scholz and Qiang Wang for their technical help with the model FESOM-ECHAM6, and thank Stefanie Klebe, Paul Gierz and Jiping Liu for very useful discussions and comments. This work is funded by China Scholarship Council (CSC).

References

Alam, A. and Curry, J.: Evolution of new ice and turbulent fluxes over freezing winter leads, J. Geophys. Res., 103, 15783–15802, 1998. 2153

ESDD
6, 2137–2179, 2015

Berger, A.: Long-term variations of daily insolation and Quaternary climatic changes, J. Atmos. Sci., 35, 2362–2367, 1978. 2146

Biggs, N., Maqueda, M. M., and Willmott, A.: Polynya flux model solutions incorporating a parameterization for the collection thickness of consolidated new ice, J. Geophys. Res., 408, 179–204, 2000. 2140, 2153

Bitz, C., Holland, M., Weaver, A., and Eby, M.: Simulating the ice-thickness distribution in a coupled climate model, J. Geophys. Res., 106, 2441–2463, 2001. 2154

Chylek, P., Folland, C., Lesins, G., Dubey, M., and Wang, M.: Arctic air temperature change amplification and the Atlantic multidecadal oscillation, Geophys. Res. Lett., 36, 14, doi:10.1029/2009GL038777, 2009. 2155

Crucifix, M., Braconnot, P., Harrison, S., and Otto-Bliesner, B.: Second phase of paleoclimate modelling intercomparison project, Eos, Trans. Amer. Geophys. Union, 86, 264–264, 2005. 2146

Danilov, S., Kivman, G., and Schröter, J.: A finite element ocean model: principles and evaluation, Ocean Model., 6, 125–150, 2004. 2143

Deser, C., Tomas, R., Alexander, M., and Lawrence, D.: The seasonal atmospheric response to projected Arctic sea ice loss in the late twenty-first century, J. Climate, 23, 333–351, doi:10.1175/2009JCLI3053.1, 2010. 2139

Dorn, W., Dethloff, K., and Rinke, A.: Improved simulation of feedbacks between atmosphere and sea ice over the Arctic Ocean in a coupled regional climate model, Ocean Model., 29, 103–114, 2009. 2140, 2141, 2142, 2143

Dumont, D., Kohout, A., and Bertino, L.: A wave-based model for the marginal ice zone including a floe breaking parameterization, J. Geophys. Res., 116, C4, doi:10.1029/2010JC006682, 2011. 2155

Fichefet, T. and Maqueda, M.: Sensitivity of a global sea ice model to the treatment of ice thermodynamics and dynamics, J. Geophys. Res.-Oceans, 102, 12609–12646, 1997. 2140, 2153

Gerdes, R.: Atmospheric response to changes in Arctic sea ice thickness, Geophys. Res. Lett., 33, 18, doi:10.1029/2006GL027146, 2006. 2155

Graf, H.-F., Perlwitz, J., Kirchner, I., and Schult, I.: Recent northern winter climate trends, ozone changes and increased greenhouse gas forcing, Contrib. Atmos. Phys., 68, 233–248, 1995. 2155

ESDD
6, 2137–2179, 2015

Hibler, W.: A dynamic thermodynamic sea ice model, J. Phys. Oceanogr., 9, 815–846, 1979. 2140, 2141, 2142, 2143, 2152
Hunke, E. and Dukowicz, J.: An elastic-viscous-plastic model for sea ice dynamics, J. Phys. Oceanogr., 27, 1849–1868, 1997. 2143
Hurrell, J. W.: Decadal trends in the North Atlantic Oscillation: regional temperatures and precipitation, Science, 269, 676–679, 1995. 2151, 2155
IPCC: Climate change 2013: the physical science basis. Contribution of working group I to the fifth assessment report of the intergovernmental panel on climate change, 2013. 2139
Juricke, S. and Jung, T.: Influence of stochastic sea ice parametrization on climate and the role of atmosphere–sea ice–ocean interaction, Philos. T. R. Soc. A, 372, 20130283, doi:10.1098/rsta.2013.0283, 2014. 2157
Kämpf, J. and Backhaus, J.: Ice-ocean interactions during shallow convection under conditions of steady winds: three-dimensional numerical studies, Deep-Sea Res., 46, 1335–1355, 1999. 2153
Knight, J., Allan, R., Folland, C., Vellinga, M., and Mann, M.: A signature of persistent natural thermohaline circulation cycles in observed climate, Geophys. Res. Lett., 32, 20, doi:10.1029/2005GL024233, 2005. 2155
Kodera, K. and Koide, H.: Spatial and seasonal characteristics of recent decadal trends in the northern hemispheric troposphere and stratosphere, J. Geophys. Res., 102, 19433–19447, 1997. 2155
Kodera, K. and Yamazaki, K.: A possible influence of recent polar stratospheric coolings on the troposphere in the Northern Hemisphere winter, Geophys. Res. Lett., 21, 809–812, 1994. 2155
Koenigk, T., Mikolajewicz, U., Jungclaus, J. H., and Kroll, A.: Sea ice in the Barents Sea: seasonal to interannual variability and climate feedbacks in a global coupled model, Clim. Dynam., 32, 1119–1138, 2009. 2155
Leppäranta, M.: A growth model for black ice, snow ice, and snow thickness in subarctic basins, Nord. Hydrol., 14, 59–70, 1983. 2143
Lohmann, G. and Gerdes, R.: Sea Ice Effects on the Sensitivity of the Thermohaline Circulation, J. Climate, 11, 2789–2803, 1998. 2155
Lohmann, G., Haak, H., and Jungclaus, J. H.: Estimating trends of Atlantic meridional overturning circulation from long-term hydrographic data and model simulations, Ocean Dynam., 58, 127–138, doi:10.1007/s10236-008-0136-7, 2008. 2155

ESDD
6, 2137–2179, 2015

Martin, S. and Kaufmann, P.: A field and laboratory study of wave damping by grease ice, J. Glaciol., 27, 283–313, 1981. 2153
Maykut, G. A.: The surface heat and mass balance, Springer, 1986. 2153
Maykut, G. A. and Untersteiner, N.: Some Results from a Time-Dependent thermodynamic Model of sea ice, J. Geophys. Res., 76, 1550–1575, 1971. 2145
Mellor, G. and Kantha, L.: An ice-ocean coupled model, J. Geophys. Res., 94, 10937–10954, 1989. 2140
Notz, D.: Challenges in simulating sea ice in Earth System Models, Wiley Interdisciplinary Reviews: Climate Change, 3, 509–526, doi:10.1002/wcc.189, 2012. 2139, 2140, 2152
Owens, W. and Lemke, P.: Sensitivity studies with a sea ice-mixed layer-pycnocline model in the Weddel Sea, J. Geophys. Res., 95, 9527–9538, 1990. 2143
Parkinson, C. and Washington, W.: A large-scale numerical model of sea ice, J. Geophys. Res., 84, 311–337, 1979. 2143
Perovich, D., Grenfell, T., Light, B., Richter-Menge, J., Sturm, M., Tucker III, W., Eicken, H., Maykut, G., and Elder, B.: SHEBA: Snow and ice studies [CD-ROM], US Army Cold Reg. Res. and Eng. Lab, 1999. 2144
Redi, M.: Oceanic isopycnal mixing by coordinate rotation, J. Phys. Oceanogr., 12, 1154–1158, 1982. 2143
Royer, J., Planton, S., and Déqué, M.: A sentitivity experiment for the removal of Arctic sea ice with the French spectral general circulation model, Clim. Dynam., 5, 1–17, doi:10.1007/BF00195850, 1990. 2139
Rühlemann, C., Mulitza, S., Lohmann, G., Paul, A., Prange, M., and Wefer, G.: Intermediate depth warming in the tropical Atlantic related to weakened thermohaline circulation: Combining paleoclimate and modeling data for the last deglaciation, Paleoceanography, 19, 1, doi:10.1029/2003PA000948, 2004. 2155
Scholz, P., Lohmann, G., Wang, Q., and Danilov, S.: Evaluation of a Finite-Element Sea-Ice Ocean Model (FESOM) set-up to study the interannual to decadal variability in the deep-water formation rates, Ocean Dynam., 63, 347–370, 2013. 2143
Semmler, T., McGrath, R., and Wang, S.: The impact of Arctic sea ice on the Arctic energy budget and on the climate of the Northern mid-latitides, Clim. Dynam., 39, 2675–2694, doi:10.1007/s00382-012-1353-9, 2012. 2139, 2155
Semtner, A.: A model for the thermodynamic growth of sea ice in numerical investigations of climate, J. Phys. Oceanogr., 6, 379–389, 1976. 2143, 2144

ESDD
6, 2137–2179, 2015

Sidorenko, D., Wang, Q., Danilov, S., and Schröter, J.: FESOM under coordinated ocean-ice reference experiment foring, Ocean Dynam., 61, 881–890. doi:10.1007/s10236-011-0406-7, 2011. 2143, 2152

Sidorenko, D., Rackow, T., Jung, T., Semmler, T., Barbi, D., Danilov, S., Dethloff, W., Dorn, K., Fieg, K., Goessling, H. F., Handorf, D., Harig, S., Hiller, W., Juricke, S., Losch, M., Schröter, J., Sein, D. V., and Wang, Q.: Towards multi-resolution global climate modeling with ECHAM6-FESOM. Part I: Model formulation and mean climate, Clim. Dynam., 44, 757–780, doi:10.1007/s00382-014-2290-6, 2014. 2140, 2143, 2147, 2154

Smedsrud, L.: Grease-ice thickness parameterization, Ann. Glaciol., 52, 77–82, 2011. 2140, 2153

Smedsrud, L. and Skogseth, R.: Field measurements of Arctic grease ice properties and processes, Cold Reg. Sci. Technol., 44, 171–183, 2006. 2153

Stevens, B., Giorgetta, M., Esch, M., Mauritsen, T., Crueger, T., Rast, S., Salzmann, M., Schmidt, H., Bader, J., Block, K., Brokopf, R., Fast, I., Kinne, S., Kornblueh, L., Lohmann, U., Pincus, R., Reichler, T., and Roeckner, E.: Atmospheric component of the MPI-M Earth System Model: ECHAM6, J. Adv. Model. Earth Syst., 5, 1–27, doi:10.1002/jame.20015, doi:10.1002/jame.20015, 2013. 2143

Timmermann, R., Danilov, S., Schröter, J., Böning, C., Sidorenko, D., and Rollenhagen, K.: Ocean circulation and sea ice distribution in a finite element global sea ice-ocean model, Ocean Model., 27, 114–129, 2009. 2143

Vancoppenolle, M., Fichefet, T., Goosse, H., Bouillon, S., Madec, G., and Maqueda, M. A. M.: Simulating the mass balance and salinity of Arctic and Antarctic sea ice. 1. Model description and validation, Ocean Model., 27, 33–53, 2009. 2140, 2153

Wang, Q., Danilov, S., Sidorenko, D., Timmermann, R., Wekerle, C., Wang, X., Jung, T., and Schröter, J.: The Finite Element Sea Ice-Ocean Model (FESOM) v.1.4: formulation of an ocean general circulation model, Geosci. Model Dev., 7, 663–693, doi:10.5194/gmd-7-663-2014, 2014. 2143

Wang, Z., Lu, Y., Wright, D. G., and Dupont, F.: Sea ice sensitivity to the parameterisation of open water area, J. Oper. Oceanogr., 3, 3–9, 2010. 2140, 2153

Winsor, P. and Björk, G.: Polynya activity in the Arctic Ocean from 1958–1997, J. Geophys. Res., 105, 8789–8803, 2000. 2153

ESDD
6, 2137–2179, 2015

Zhang, R.: Can the Atlantic Ocean drive the observed multidecadal variability in Northern Hemisphere mean temperature?, Geophys. Res. Lett., 34, 2, doi:10.1029/2006GL028683, 2007. 2155

Zhang, R.: Coherent surface-subsurface fingerprint of the Atlantic meridional overturning circulation, Geophys. Res. Lett., 35, 20, doi:10.1029/2008GL035463, 2008. 2155

ESDD

6, 2137–2179, 2015

Table 1. List of variables.

Name	Description	Value
A	ice concentration	
$\dot{A}_{\mathrm{ice}}$	decrease rate of ice concentration induced by vertical melting	
$\dot{A}_{\mathrm{ow}}$	increase rate of ice concentration induced by freezing on open water	
c_{w}	specific heat capacity of sea water	$4190\,\mathrm{J\,kg^{-1}\,K}$
c_*	factor for changing lead closing parameter	
F_{atmice}	heat flux at air-ice interface	
F_{atmocn}	heat flux at air-ocean interface	
F_{ocnice}	heat flux at ice-ocean interface	
h	grid-cell mean ice thickness	
h'	actual ice thickness	
h_{mix}	depth of ocean mixed layer	40 m
h_0	lead closing parameter or demarcation thickness between thin and thick ice	
h_0^{max}	maximum threshold of demarcation ice thickness	1.5 m
h_0^{min}	minimum threshold of demarcation ice thickness	0.5 m
$\dot{h}_{\mathrm{ice}}$	thermodynamic ice production rate at ice-covered area	
$\dot{h}_{\mathrm{ow}}$	thermodynamic ice production rate at open water area	
L	latent heat of fusion	$3.34 \times 10^5\,\mathrm{J\,kg^{-1}}$
T_{f}	freezing temperature of sea water	$-1.836\,^{\circ}\mathrm{C}$
T_{s}	temperature of ice surface	
γ_{t}	heat transfer rate in the ice-ocean interface	$10/86\,400\,\mathrm{m\,s^{-1}}$
δt	time step	
ρ_{i}	density of sea ice	$910\,\mathrm{kg\,m^{-3}}$
ρ_{w}	density of sea water	$1025\,\mathrm{kg\,m^{-3}}$

ESDD
6, 2137–2179, 2015

Table 2. List of experiments. FE* stands for experiments performed by FESOM-ECHAM6; SIM* refers to simulations by the SIM. CTR stands for the control experiment.

Name	Description
FE-CTR	Use Eq. (1).
FE80	Use Eq. (6), $c_* = 80f$.
SIM-CTR	Use Eq. (1)
SIM80	Use Eq. (6), $c_* = 80\,\%$.
SIM60	Use Eq. (6), $c_* = 60\,\%$.
SIM40	Use Eq. (6), $c_* = 40\,\%$.
SIM20	Use Eq. (6), $c_* = 20\,\%$.

ESDD
6, 2137–2179, 2015

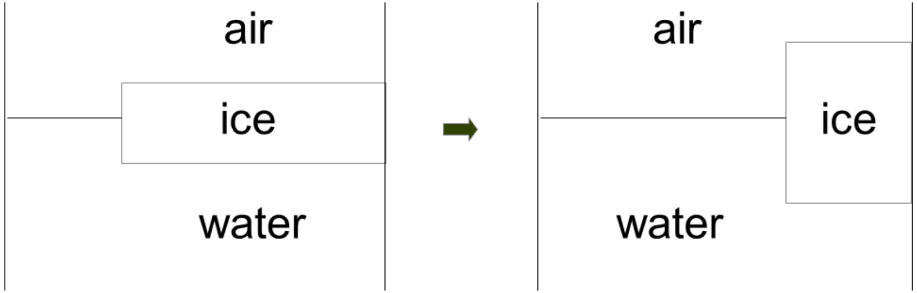

Figure 1. Two different kinds of newborn ice on open water. Left panel shows ice with actual thickness h_1 and area A_1, right panel shows ice with actual thickness h_2 and area A_2 ($h_2 > h_1, A_2 < A_1$), and $h_1 A_1 = h_2 A_2$.

ESDD
6, 2137–2179, 2015

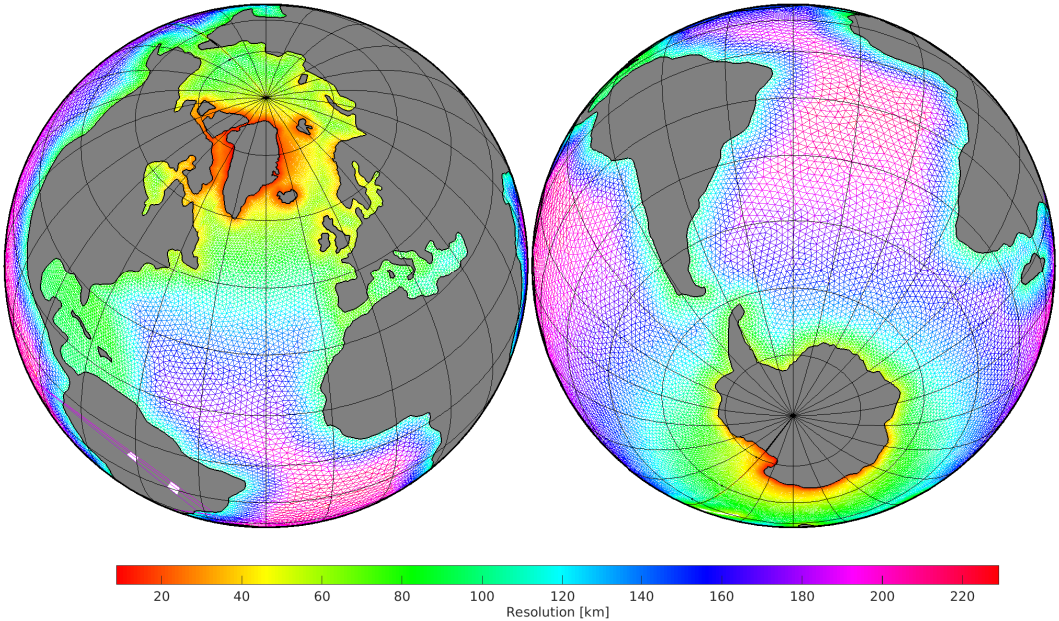

Figure 2. FESOM mesh resolution applied in our experiments.

ESDD
6, 2137–2179, 2015

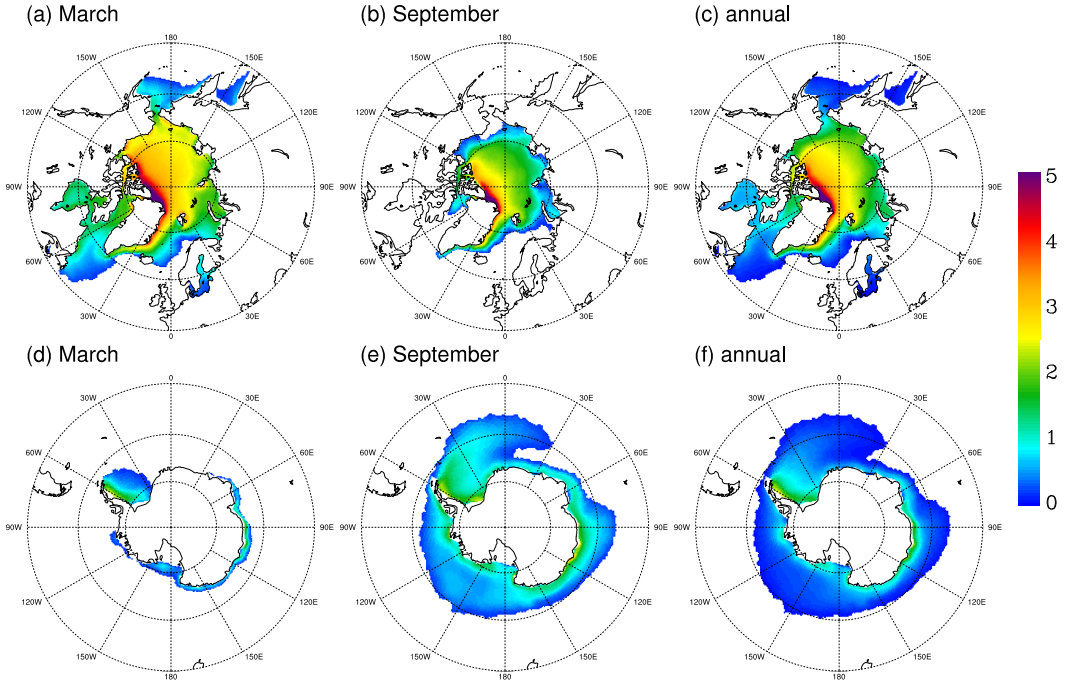

Figure 3. Sea ice thickness for FE-CTR, units are m.

ESDD
6, 2137–2179, 2015




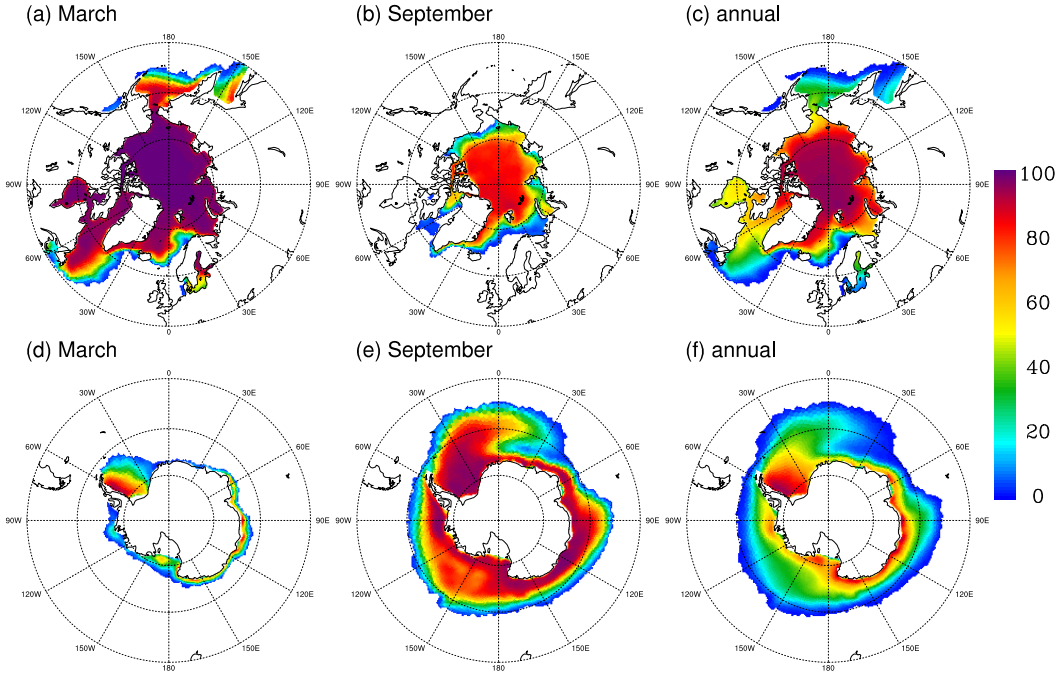

Figure 4. As in Fig. 3, but for sea ice concentration, units are %.

ESDD
6, 2137–2179, 2015

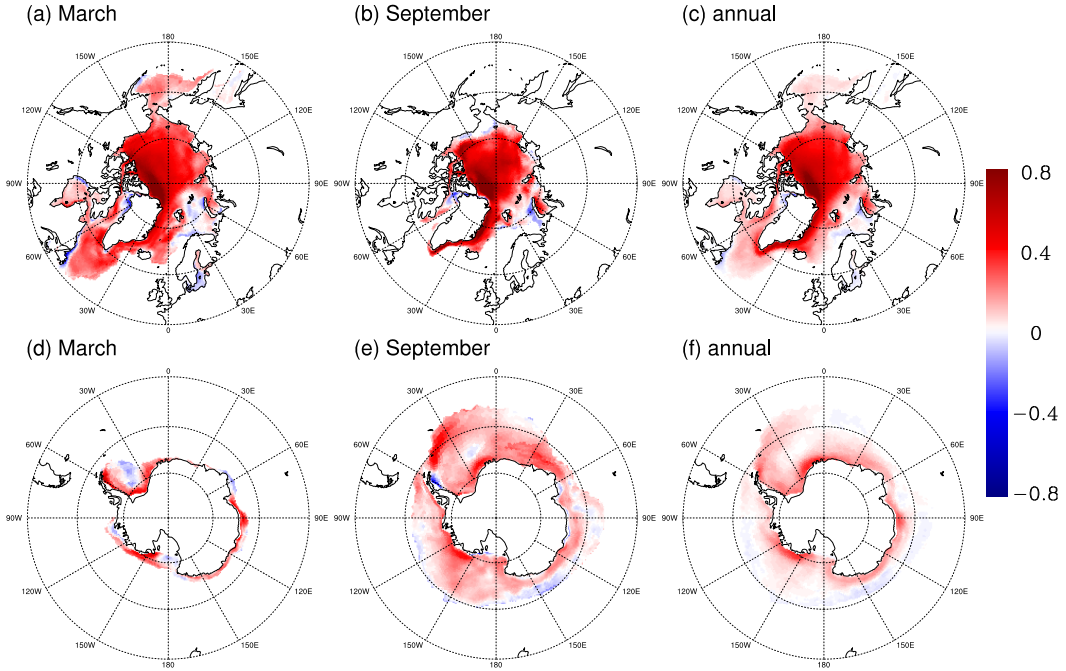

Figure 5. Sea ice thickness amomalies of FE80 compared to FE-CTR, units are m.

ESDD
6, 2137–2179, 2015

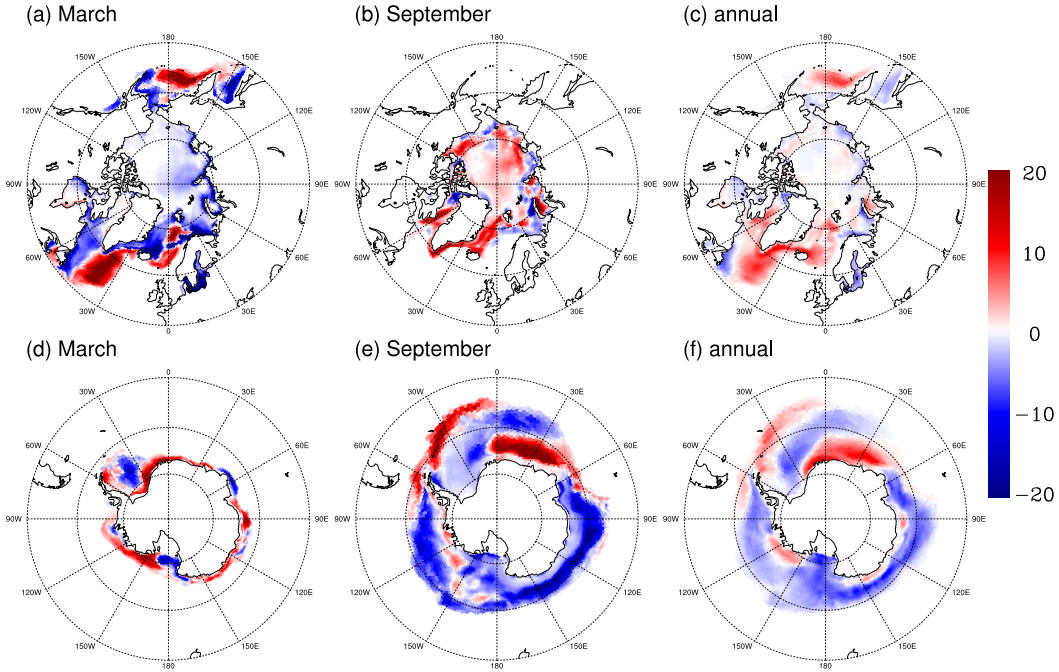

Figure 6. As in Fig. 5, but for sea ice concentration, units are %.

ESDD
6, 2137–2179, 2015

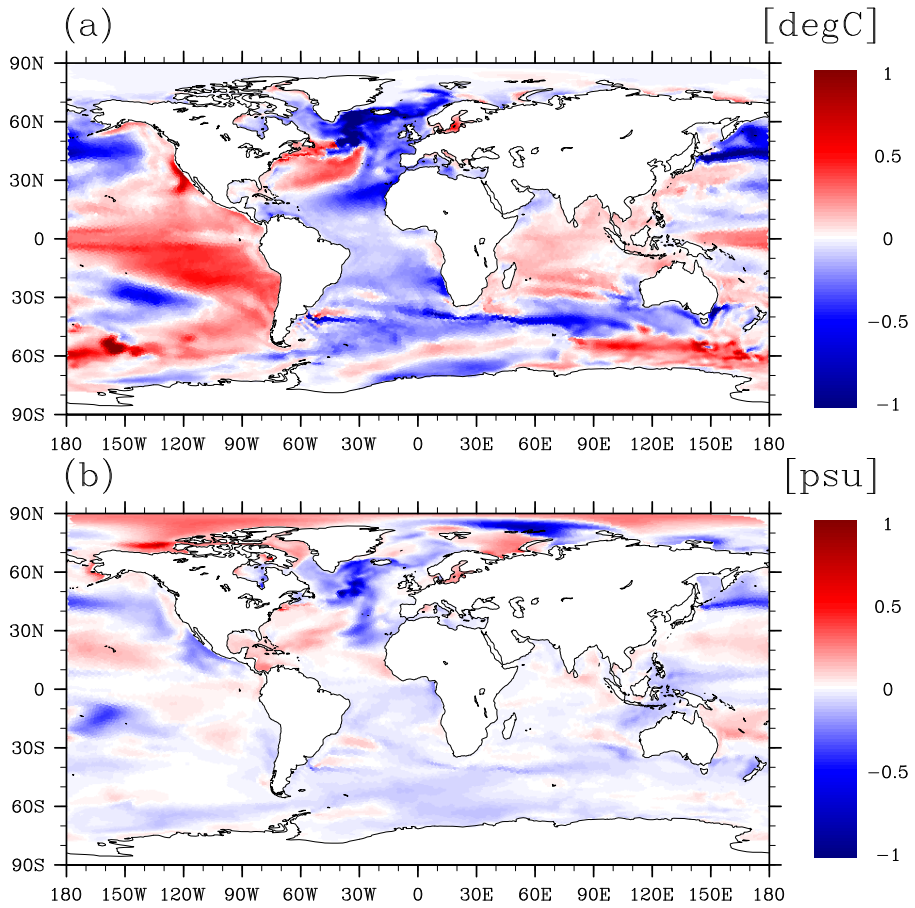

Figure 7. Difference of annual mean **(a)** the sea surface temperature and **(b)** the sea surface salinity between experiments FE80 and FE-CTR (FE80 minus FE-CTR).

ESDD
6, 2137–2179, 2015

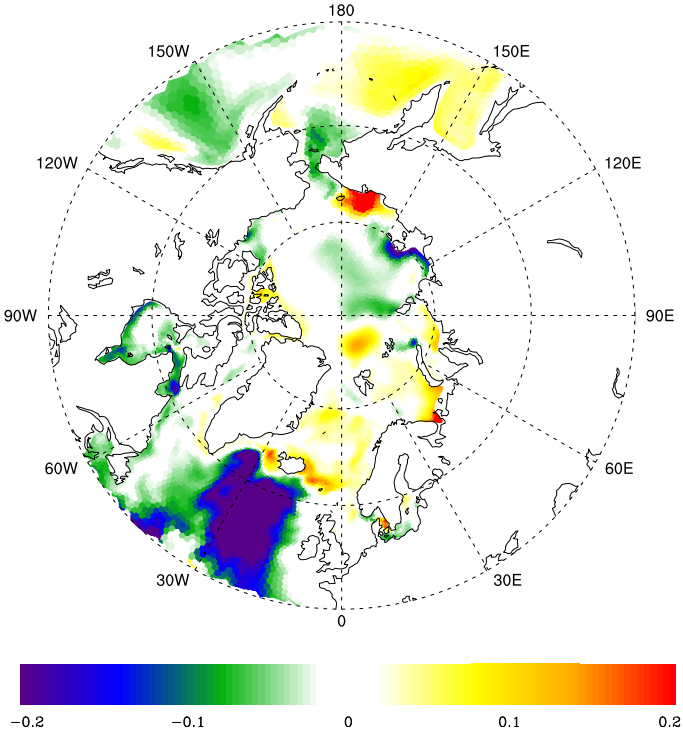

Figure 8. Composite map between sea surface salinity anomalies and high Fram Strait ice mass import with a lag of −4 years. Units are psu. Composite map shown here is calculated by subtracting the slices that are above one standard deviation of the indices of Fram Strait ice mass import.

ESDD
6, 2137–2179, 2015

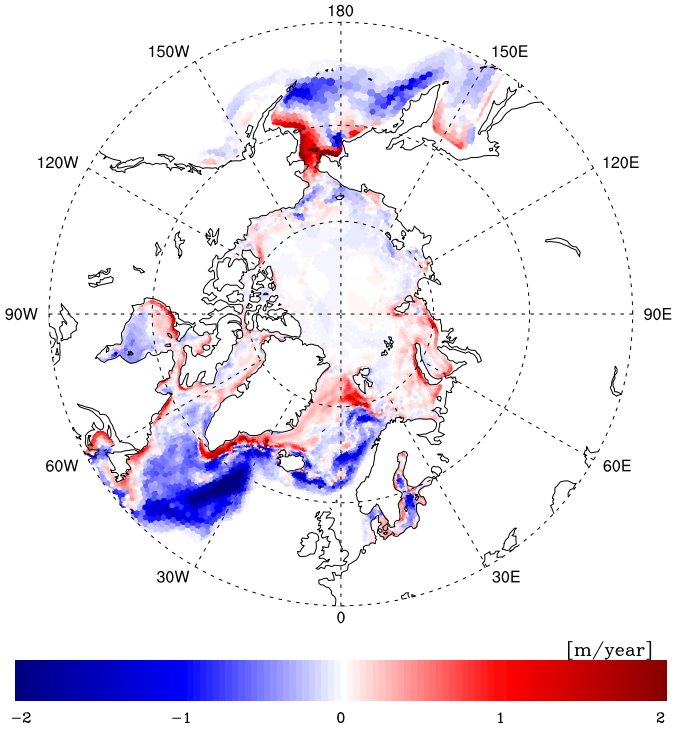

Figure 9. Difference of annual mean thermodynamic growth rate of grid-cell mean ice thickness between experiments FE80 and FE-CTR (FE80 minus FE-CTR).

ESDD
6, 2137–2179, 2015

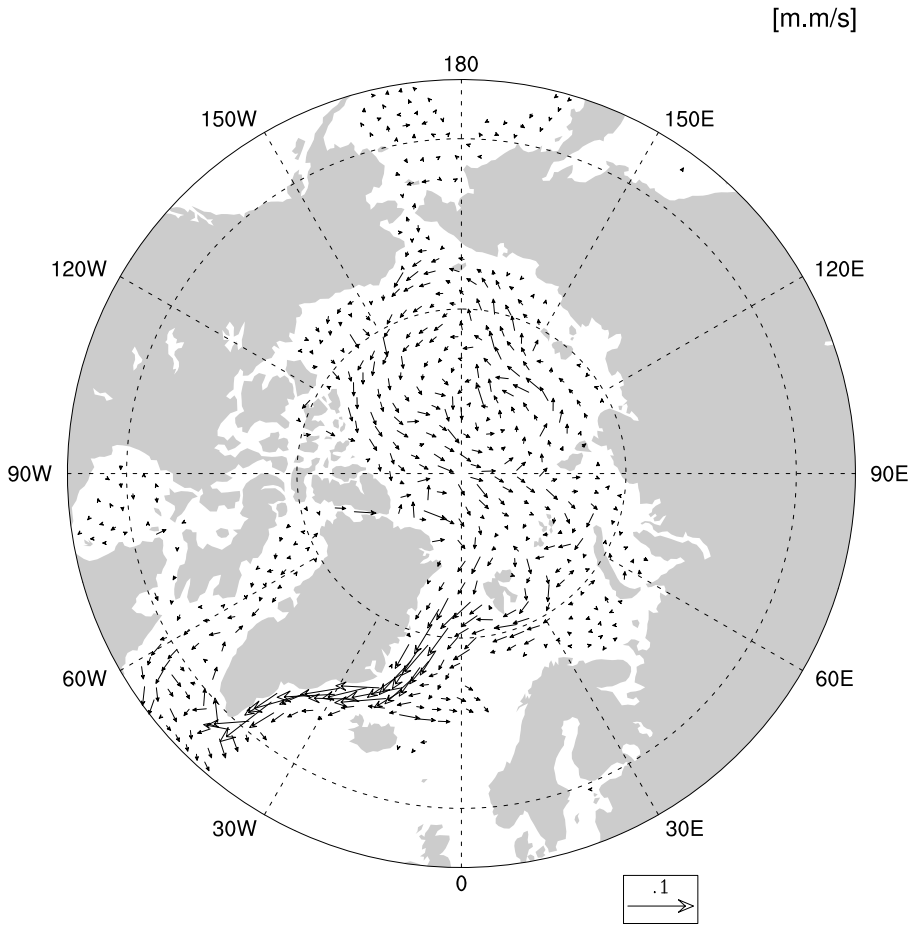

Figure 10. Simulated anomalies of annual mean ice mass transport between experiments FE80 and FE-CTR (FE80 minus FE-CTR). Units are $m^2\ s^{-1}$.

ESDD
6, 2137–2179, 2015

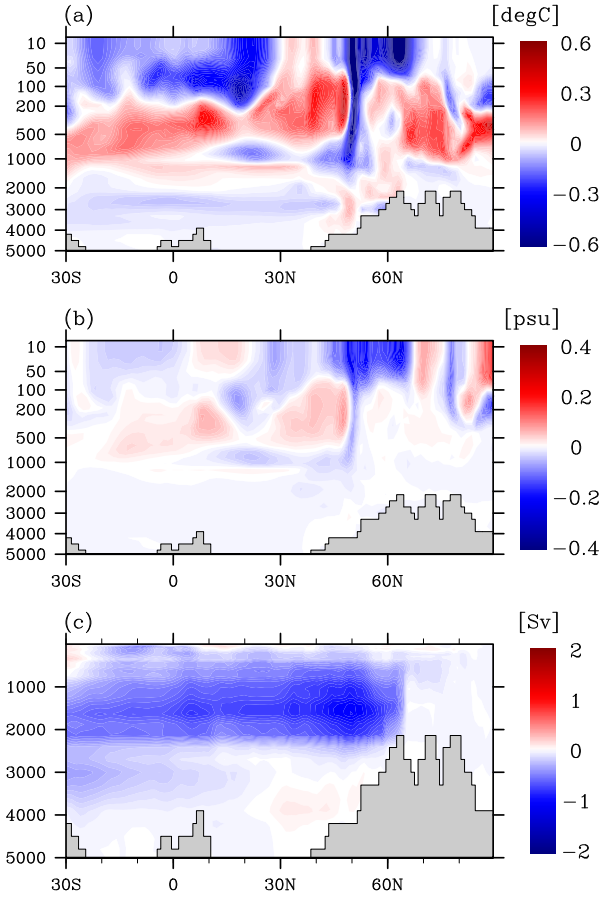

Figure 11. Difference of **(a)** zonal mean ocean temperature, **(b)** zonal mean ocean salinity and **(c)** AMOC between experiments FE80 and FE-CTR (FE80 minus FE-CTR) for the Atlantic region.

ESDD
6, 2137–2179, 2015

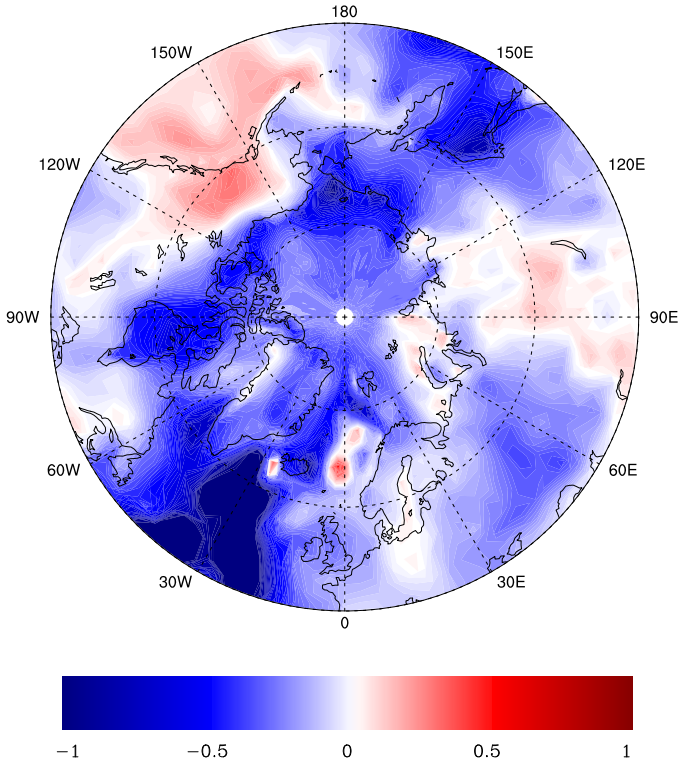

Figure 12. Composite map between surface air temperature anomalies and low phases of AMOC. Units are ˚C. Composite map shown here is calculated by subtracting the fields that are below one standard deviation of the AMOC indices.

ESDD
6, 2137–2179, 2015

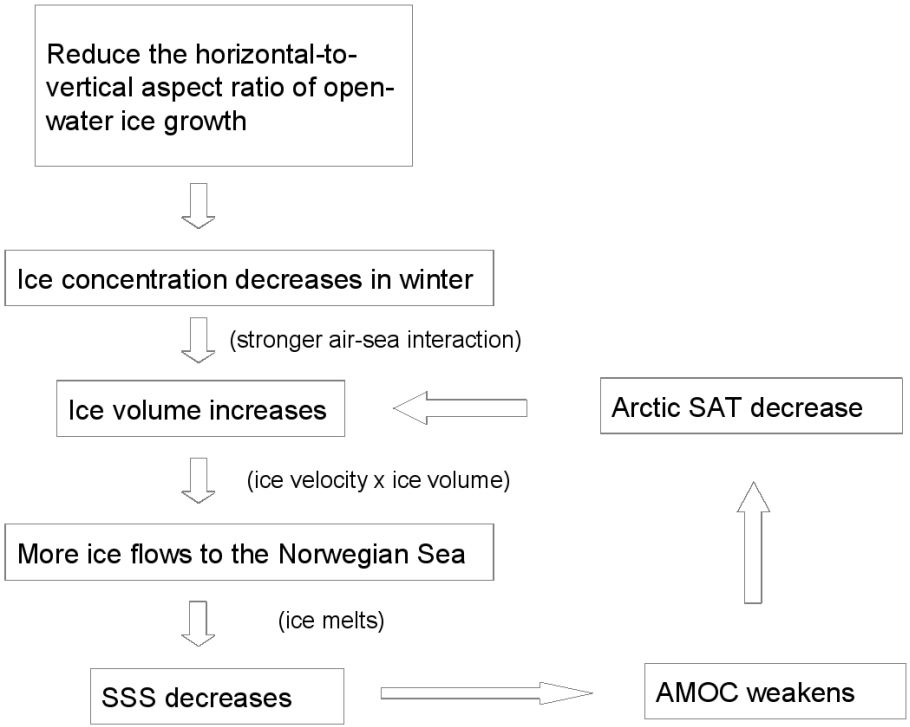

Figure 13. Positive feedback in the Northern Hemisphere between sea ice and large-scale ocean circulation.

ESDD
6, 2137–2179, 2015

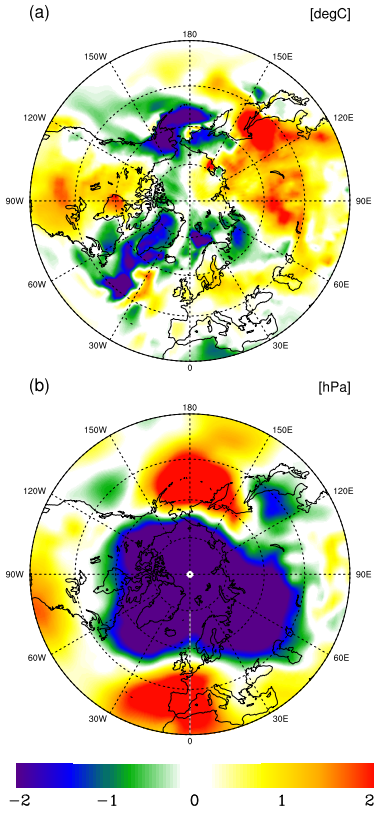

Figure 14. Difference of **(a)** surface air temperature and **(b)** sea level pressure in boreal winter between experiments FE80 and FE-CTR (FE80 minus FE-CTR). Units are ˚C and hPa.

ESDD
6, 2137–2179, 2015

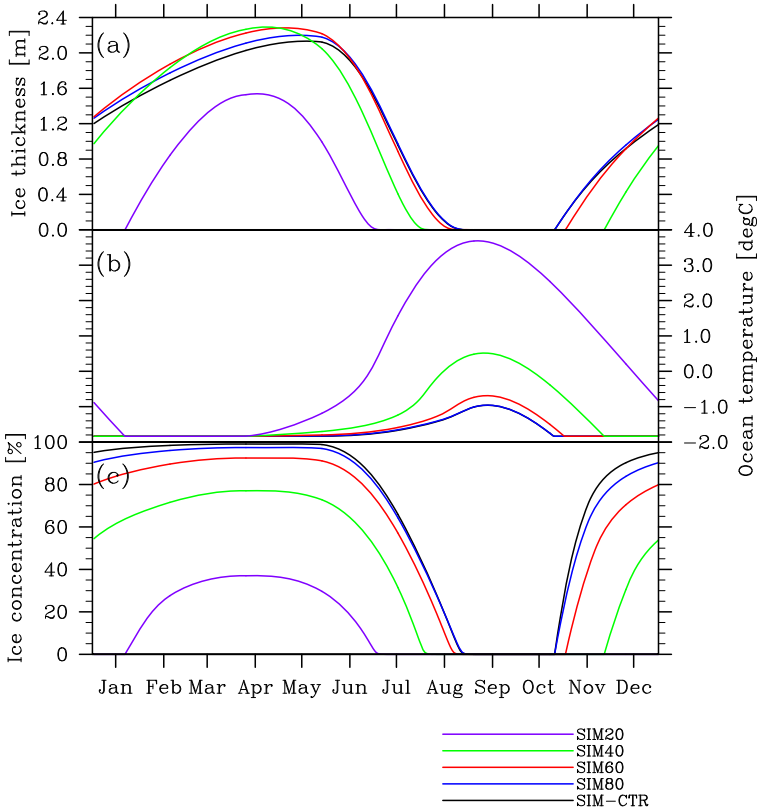

Figure 15. Time series of **(a)** sea-ice thickness, **(b)** ocean temperature and **(c)** sea-ice concentration in the experiments SIM-CTR, SIM80, SIM60, SIM40 and SIM20. The model is run into equilibrium.

ESDD
6, 2137–2179, 2015